IEEE Photonics Journal
An IEEE Photonics Society Publication

Dynamic Intermode Beat Frequency Control of an Optical Frequency Comb Single Section Quantum Dot Laser by Dual-Cavity Optical Self-Injection

Volume 11, Number 5, October 2019

Sebastian Stutz
Dominik Auth
Christoph Weber
Lukas Drzewietzki
Oleg Nikiforov
Ricardo Rosales
Thomas Walther
Luke F. Lester, *Fellow, IEEE*
Stefan Breuer, *Member, IEEE*

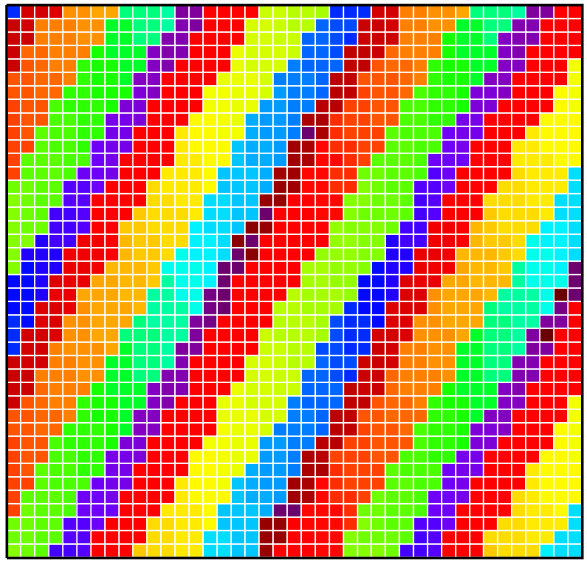

DOI: 10.1109/JPHOT.2019.2932452

IEEE photonics SOCIETY

IEEE

Dynamic Intermode Beat Frequency Control of an Optical Frequency Comb Single Section Quantum Dot Laser by Dual-Cavity Optical Self-Injection

Sebastian Stutz,[1] Dominik Auth,[1] Christoph Weber,[1] Lukas Drzewietzki,[1] Oleg Nikiforov,[1] Ricardo Rosales,[2] Thomas Walther,[1] Luke F. Lester,[3] *Fellow, IEEE*, and Stefan Breuer,[1] *Member, IEEE*

[1]Institut für Angewandte Physik, Technische Universität Darmstadt, 64289 Darmstadt, Germany
[2]Institut für Festkörperphysik, Technische Universität Berlin, 10623 Berlin, Germany
[3]Department of Electrical and Computer Engineering, Virginia Tech, Blacksburg, VA 24061 USA

DOI:10.1109/JPHOT.2019.2932452

Manuscript received July 19, 2019; accepted July 28, 2019. Date of publication August 1, 2019; date of current version September 23, 2019. This work was supported in part by the DFG under Grant 389193326 and in part by the Open Access Publishing Fund of TU Darmstadt for article processing charge. The work of D. Auth was supported by the doctoral fellowship funded by the Adolf Messer Foundation. The work of L. F. Lester and S. Breuer was supported by the TU Darmstadt (Department International Affairs). Corresponding author: Stefan Breuer (e-mail: stefan.breuer@physik.tu-darmstadt.de).

Abstract: Dynamic frequency tuning of the 40.67 GHz intermode beat frequency of a 1255 nm emitting 1 mm long monolithic self mode-locked single section optical frequency comb InAs/InGaAs quantum dot laser across 70 MHz is experimentally demonstrated by fine-delay dual-cavity controlled all optical self-injection. Fiber-based macroscopic optical delay lengths are 9.4 m (round-trip time of 62.7 ns) and 16.5 m (round-trip time of 110.1 ns), the maximum studied microscopic delay tuning times are 40 ps and the optical self-injection strengths are below 0.02%. For selected delay times, the lowest intermode beat frequency line width amounts to 2 kHz indicating an improvement of carrier phase coherence by a factor of 700 as compared to the free-running laser. We validate these experimental results by a simple and universal stochastic time-domain model which is applied for the first time to model a self mode-locked quantum dot laser subject to optical self-injection. Modeling results are in good quantitative agreement.

Index Terms: Optical frequency comb laser, quantum dot lasers, self mode-locking, intermode beat frequency, self-injection, stochastic modelling, time-domain modelling.

1. Introduction

Optical frequency comb (OFC) self mode-locked (SML) semiconductor lasers are compact monolithic photonic sources providing a large number of mutually locked optical carriers for application as coherent multi-frequency super-channel sources in high data rate optical communication [1]–[4] or dual-comb spectroscopy [5]. There, a high degree of coherence between the carriers, indicated by a stable comb line spacing or intermode beat frequency (IBF) is demanded. SML laser emission in the mid-infrared has been recently reported for quantum cascade lasers [5], [6]. In the

near-infrared SML laser emission has been demonstrated for quantum dot [7]–[10], quantum dash [3], [4], [11]–[20] and quantum well [21], [22] active regions spanning wavelengths from 1250 nm to 1585 nm. Intermode beat line widths (IBLWs) range from sub-kHz to a few hundreds of kHz and the mode (carrier) spacing from 4.4 GHz (10 mm long monolithic cavity) [18] to 134 GHz (0.34 mm long cavity) [19]. The IBF timing phase noise stability, directly correlated to the IBLW of a mode-locked semiconductor laser [23], indicates the degree of phase coherence between the OFC carriers. It can be optimized by laser cavity design or improved by multi-section cavity layout and laser biasing [24]–[27], passive electrical stabilization [28], [29] or by external control including active mode-locking [30]–[33], electrical modulation or hybrid mode-locking [31], [34], single- and dual-mode injection [35], [36] or mutual synchronization [37]. Self-injection by single passive external cavities [2], [4], [17], [20], [38]–[44] allows to effectively control the IBF and IBLW of mode-locked semiconductor lasers in a frequency range depending on the length of the external cavity [44]. Optical self-injection (OSI) however induces time-delay signature sidebands in the radio-frequency (RF) spectrum which on the other hand can be effectively suppressed by dual-cavity OSI as suggested experimentally [45], [46] and confirmed theoretically by modeling [46]–[48]. The simultaneous IBF control and full suppression of RF sidebands of OFCs generated by quantum dot SML semiconductor lasers by dual-cavity OSI has yet not been experimentally or numerically demonstrated.

In this work, the dynamic IBF control of a monolithic InAs/InGaAs quantum dot laser emitting an OFC centered at 1250 nm is demonstrated experimentally and confirmed by modeling. Two macroscopic external passive optical cavities with individual microscopic fine-delay allow to dynamically control the IBF. We quantify the improvement in timing stability by IBLW measurements and confirm these experimental results by an universal stochastic model.

2. Laser Structure and Experimental Setup

The monolithic laser consists of 10 layers of InGaAs/GaAs quantum dots embedded in a 440 nm GaAs waveguide surrounded with $Al_{0.35}$ $Ga_{0.65}$ As claddings [49]. The Fabry-Perot cavity is 1 mm long corresponding to an internal round trip time $T_0 = 25$ ps. The ridge width is 6 μm and the facets are as cleaved. The laser is biased at 180 mA by a low-noise current source and is stabilized at a laser cooling block temperature of 20 °C. It emits 16 comb lines within a -3 dB spectral width of 3.5 nm at 1255 nm. The comb line spacing of the free-running laser amounts to $IBF_{0,exp} = 40.6707$ GHz. An optical pulse width of 2 ps (external chirp compensated) is verified by nonlinear intensity optical autocorrelation, while in this work the laser pulses are strongly chirped and the laser emits a continuous-wave output in frequency-modulated mode-locking operation [50]. A schematic of the developed experimental dual-cavity OSI setup is illustrated in Fig. 1. The OFC quantum dot laser emission is collimated and two beams, separated by free space beam splitters, are coupled into two single-mode fibers (SMFs) by aspheric lenses. The fiber outputs are collimated and directed towards two high-reflective mirrors that are mounted on two motorized high-precision linear translation stages. The fiber-based fixed macroscopic delay amounts to 9.4 m optical path length for the shorter fiber cavity L_1, corresponding to a frequency of $f_1 = 16$ MHz or cavity round-trip times of $\tau_1 = 2508 \times T_0 = 62.7$ ns, and 16.5 m optical path length for the longer fiber cavity L_2, corresponding to $f_2 = 9.1$ MHz and cavity round-trip times of $\tau_2 = 4403 \times T_0 = 110.1$ ns, respectively. The high-precision motorized stages control both time delays $L_{mic,1,2}$ in the two microscopic cavities by micrometer-resolved linear spatial mirror translations up to a maximum of 40 ps, therefore both passive optical cavities consist of total lengths $L_{1,2} = L_{mac,1,2} + L_{mic,1,2}$. The back reflected optical power is individually controlled by two variable optical attenuators. The OSI strengths are set to values of 0.018% for L_1 and 0.014% for L_2 given as the fraction of the total emitted output power coupled back onto the laser facet. These OSI strengths are sufficient to achieve a full IBF tuning range predicted by the model. Stronger OSI strengths result in higher noise induced sidebands in the RF spectrum. The OSI strengths are kept at this low values to ensure that the induced sidebands are at least 3 dB lower than the main IBF signal. Two polarization controllers ensure polarization matching of the back-reflected light and the linear polarization emitted by the laser. For emission analysis, a part of the beam is coupled

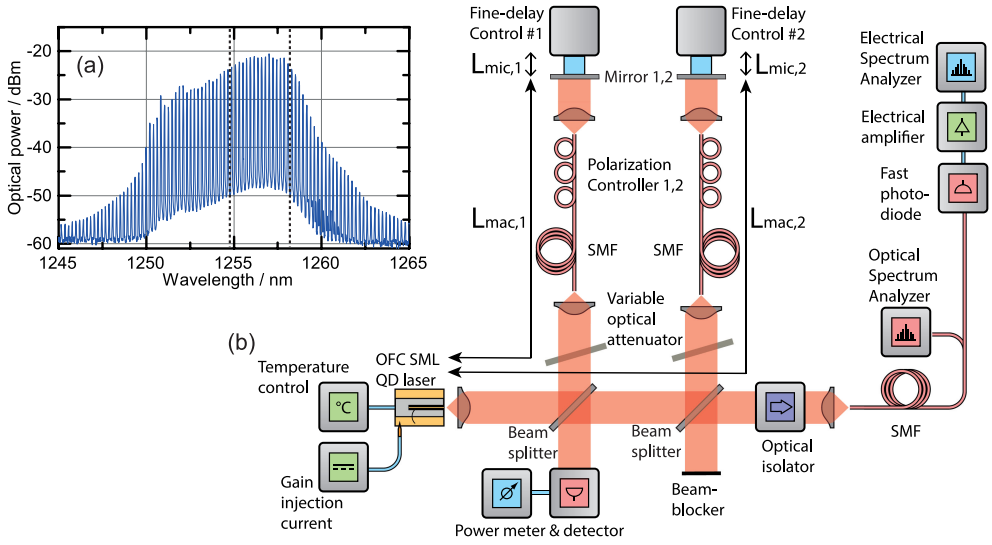

Fig. 1. (a) The OFC spectrum for an injection current of 180 mA and 20 °C. The dashed lines include the 16 comb carriers within the −3 dB spectral width. (b) Schematic depiction of the experimental setup developed for IBF control by dual-cavity OSI of a OFC quantum dot laser.

into a SMF and detected by a fiber-coupled fast photo diode (electrical bandwidth $>$ 45 GHz) and an electrical spectrum analyzer for IBF and IBLW analysis in the RF spectral domain. An optical spectrum analyzer (10 pm spectral resolution) is used for OFC measurement. An optical isolator ($>$60 dB isolation ratio) prevents undesired residual optical back-reflections from the measurement instruments. The experiment is built on an actively vibration stabilized optical table. To shield the experiment from thermal fluctuations or acoustic noise contributions, the setup is built inside a closed aluminum box cladded with sound absorbing material.

3. Stochastic Model

To validate the experimentally studied dependencies of the IBF on the fine-delays, a stochastic time domain model is employed which considers an OFC semiconductor laser as a free-running oscillator exhibiting timing deviations within each pulse round trip [43]. A main noise source causing these deviations is spontaneous emission (SE) directly coupling to the laser pulse and, thus, inducing IBF instabilities. SE is uncorrelated and therefore white in frequency. After each round-trip, the timing deviation is accumulated leading to a Wiener process or a random walk. The basic idea of the statistical effect responsible for timing phase noise improvement or timing jitter reduction follows the inequality

$$\underbrace{\left\langle \left(\Gamma_i(N)\right)^2 \right\rangle_N}_{\text{(A)}} \geq \underbrace{\left\langle \left(\frac{\Gamma_i(N) + \Gamma_i(N - N_d)}{2} \right)^2 \right\rangle_N}_{\text{(B)}} \geq \underbrace{\left\langle \left(\frac{\Gamma_1(N) + \Gamma_2(N)}{2} \right)^2 \right\rangle_N}_{\text{(C)}} \tag{1}$$

where $\Gamma_i(N)$ is a sequence of random numbers and $\langle\rangle_N$ denotes an averaging with respect to the index N. The inequality expresses that a sequence of random numbers has a larger variance than two independent sequences of random numbers [42]–[44]. Term (A) represents a free-running OFC laser with coherently locked modes, term (C) a locking of two OFC lasers. Term (B) represents an OFC laser subject to OSI. Term (B) equals (A) when the delayed part N_d of the random sequence $\Gamma_i(N)$ is zero. Term (B) converges towards (C) when N_d approaches infinity. Thus, for increasing N_d a lower variance of the random sequences and therefore an increased timing stability is expected.

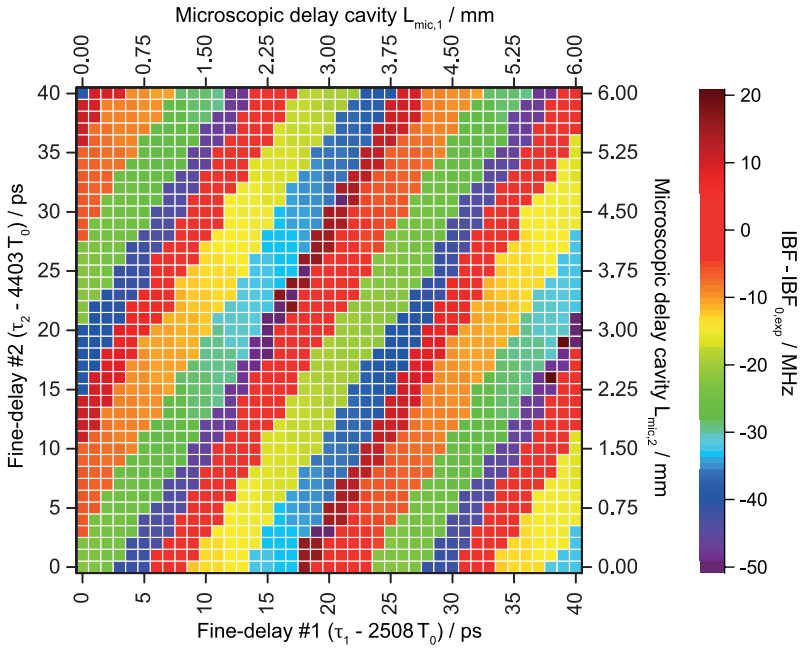

Fig. 2. Experimental results: IBF control range of the OFC quantum dot laser up to 70 MHz for fine-adjusted OSI by two passive external cavities $L_{mac,1} = 9.4$ m (2508 T_0) and $L_{mac,2} = 16.5$ m (4403 T_0). Free-running: $IBF_{0,exp} = 40.6707$ GHz.

The timing deviation T(n+1) from an ideal clock of the n+1 pulse for dual-cavity OSI hence follows

$$T(n+1) = \frac{T(n) + \sigma_{ptp}\Gamma(n) + \sum_{i=1}^{2} \gamma_i W_i(\Delta T_i) T(n - n_{d_i})}{1 + \sum_{i=1}^{2} \gamma_i W_i(\Delta T_i)} \tag{2}$$

where σ_{ptp} is the pulse-to-pulse timing jitter which is accessed by measuring the fundamental IBLW in the RF spectrum with $\sigma_{ptp} = (\Delta\nu_0/2\pi\nu_0^3)^{0.5}$ where $\Delta\nu_0$ is the -3 dB IBLWs and ν_0 the IBF [23], γ is the timing interaction strength directly correlated to the OSI strength in the experiment and n_d is the discretized time delay of the OSI in terms of number of pulses. $\Gamma(n)$ is a Gaussian distributed random number with a standard deviation of 1. The term $W_i(\Delta T_i) = W_i\big(T(n) - T(n - n_{d_i})\big)$ is a weighting pulse interaction function representing the overlap of the pulse width and the net gain window being 1 for a full overlap and 0 without overlap.

4. Experimental and Modeling Results

The experimentally attained deviations of the dual-cavity OSI IBF from the free-running IBF ($IBF_{0,exp} = 40.6707$ GHz) are depicted color-coded in Fig. 2 in dependence on both controlled microscopic delay times. The IBF increases up to 40.6907 GHz and can decrease to a minimum of 40.6207 GHz. This constitutes a continuous control range of 70 MHz. A twofold periodicity is apparent every 25 ps corresponding to the internal laser round-trip time T_0. The stripe pattern across the IBF map follows an orientation of arctan(16 MHz/9.1 MHz) $= 60^\circ$ and can be attributed to leading or trailing re-injection of the OSI laser signal into the laser cavity, whereby the IBF increases or decreases. The observed tilt stems from the stronger impact of the shorter cavity L_1 on the IBF compared to L_2, as reported for a passively mode-locked (PML) semiconductor laser [47]. Along these stripes, regimes of continuously changing IBF are evident. Within some of these regimes, the IBF abruptly transits from positive to negative deviations. This stems from the fact, that the signal-to-noise ratios of the IBF and a noise induced sideband separated by 48 MHz, corresponding to the shorter OSI cavity L_1, are below 5 dB in these transition regimes. Thus, the laser IBF transits onto this side-band.

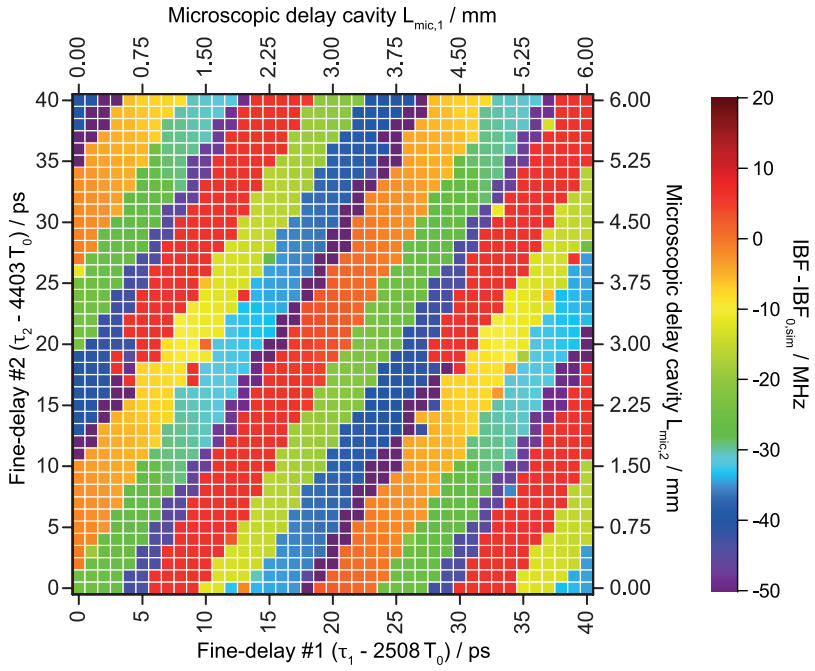

Fig. 3. Simulation results: IBF control range of the OFC quantum dot laser up to 70 MHz for fine-adjusted optical self-injection by two passive external cavities $L_{mac,1} = 9.4$ m and $L_{mac,2} = 16.5$ m. Free-running IBF = 40.67 GHz.

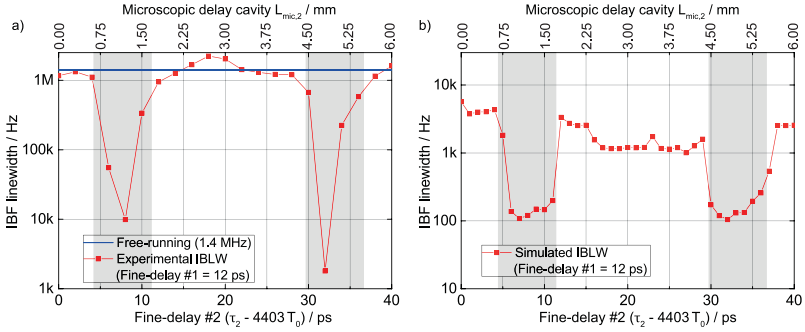

Fig. 4. (a) Experimental IBLW for a fixed fine-delay #1 at 12 ps in dependence on fine-delay #2. (b) Corresponding simulation results.

This effect is stronger in the experimental case due to the continuous tuning of the fine-delay of the cavity that causes hysteresis effects [51], whereas in the simulation each fine-delay is calculated separately. In the simulations, the external cavity round-trip frequencies are set to $f_1 = 9.1$ MHz and $f_2 = 16$ MHz corresponding to the experiment. The considered free-running IBF amounts to $IBF_{0,sim} = 40.67$ GHz and the timing interaction function W(ΔT) amounts to 8 ps to quantitatively reproduce the experimental findings. The results for the simulated IBFs are displayed in Fig. 3. An increase of the IBF of up to 20 MHz and a maximum decrease of 50 MHz can be identified. Simulations confirm the maximum control range of 70 MHz as experimentally reported. It is apparent that for specific fine-delays, few singular simulation points located at IBF transitions deviate from their nearest neighbours as well as from the experimental results. This peculiarity, for example at fine-delays $\Delta\tau_1$ of 9 ps and $\Delta\tau_2$ of 17 ps, results from the random walk nature of the underlying stochastic simulation [43]. The experimental IBLW is depicted in Fig. 4a for a fixed fine-delay #1 at 12 ps and corresponding simulation results are depicted in Fig. 4b. For specific fine-delays #2 at 8 ps and

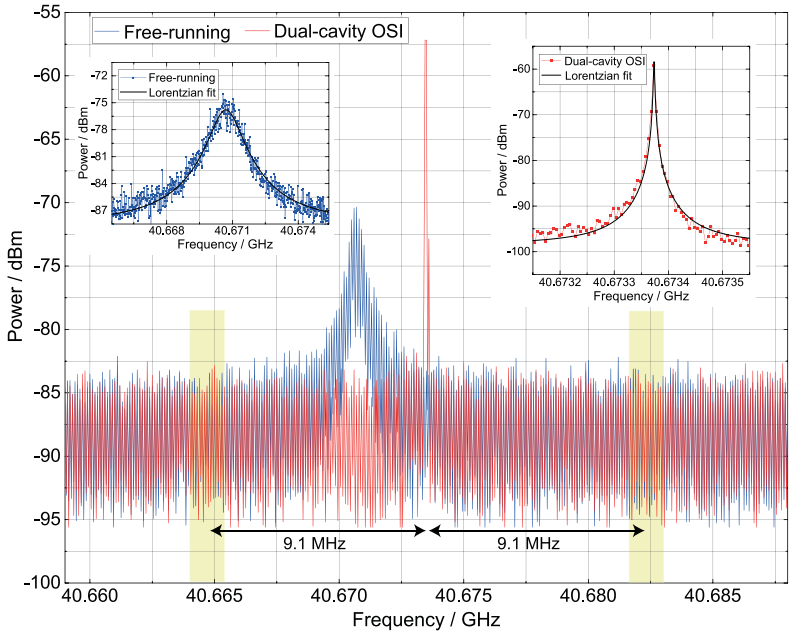

Fig. 5. Experimental results: RF spectra indicating IBLWs of 1.4 MHz (free-running, blue) and 2 kHz for dual-cavity OSI (red). Injection current 180 mA and 20 °C cooling block temperature. The insets depict zooms into IBF and Lorentzian fit for free-running operation (left) and dual-cavity OSI (right). As a guide to the eye, yellow masked frequency positions indicate where single-cavity OSI RF sideband frequencies would be expected, but are suppressed below the instruments noise floor.

32 ps, simulations indicate a minimum in IBLW. For those two delay combinations, IBLW minima are confirmed in the experiment. The overall trend predicted by the simulations is reproduced well by the experiment although simulations predict stronger IBLW reductions. This can be attributed to residual acoustic or vibration influences impacting the stability of the experimental setup. As predicted by the model, the maximum IBLW reduction is experimentally found at $\Delta\tau_1 = 12$ ps and at $\Delta\tau_2 = 32$ ps. Corresponding acquired RF spectra in free-running operation and for optimum IBLW reduction are depicted in Fig. 5 within a frequency span of 25 MHz. The IBLWs are determined by fitting the measurement data with a Lorentzian and analyzing the -3 dB width. The insets of Fig. 5 depict zooms into the acquired IBF and Lorentzian fits. Additionally, recorded timing phase noise power spectral density spectra verify the expected $1/f^2$-dependence of the timing phase noise power spectral density in dependence on the offset frequency. The IBF amounts to $\mathrm{IBF}_{0,\mathrm{exp}} = 40.6707$ GHz with a -3 dB IBLW of 1.4 MHz for free-running and approximately 40.6734 GHz with an IBLW of 2 kHz for dual-cavity OSI condition exemplifying an improvement of the IBLW by a factor of 700. Simultaneously, we confirm that potential RF sidebands, commonly induced by single-cavity OSI, are fully suppressed below the noise floor of the electrical spectrum analyzer. As a guide to the eye, the expected frequency positions of those sidebands are indicated by yellow colored masks in Fig. 5. Dual-cavity OSI annihilates the timing-noise memory of the delay by a stochastic averaging of both OSI memories. The qualitative and quantitative agreement obtained by the simple stochastic model to the experimental data in Fig. 3 suggests that the IBF of OFC emitted by the quantum dot SML semiconductor laser and the mechanism of IBLW reduction by external time-delay control appears of the same stochastic origin as demonstrated for PML lasers based on quantum dot [43] and quantum well [44] active regions. We find that the OFC stabilization in quantum dot SML lasers relies on the effective interaction of the timing of the intra-cavity laser signal and the time-delayed OSI laser signal in conjunction with a statistical averaging of the independent timing deviations of both. We can conclude that due to the strongly chirped pulses with widths being longer than their cavity roundtrip time, an interaction between intra-cavity laser signal and OSI signal is always apparent.

5. Conclusion

We demonstrated experimentally and by modeling the dynamic IBF tuning of a 1255 nm emitting 1 mm long monolithic OFC SML InAs/InGaAs quantum dot laser across 70 MHz. Fine-delay controlled dual-cavity OSI by two fiber-based macroscopic optical delay cavities of lengths 9.4 m (round-trip time of 62.7 ns) and 16.5 m (round-trip time of 110.1 ns) combined with maximum microscopic delay times of 40 ps and selected OSI strengths allowed to reduce the IBLW to 2 kHz. Modeling results obtained by a universal stochastic time-domain model confirmed quantitatively the experimentally reported range of IBF control. The same stochastic mechanism recently identified for pulse train stabilization of PML semiconductor laser by OSI appears to be underlying the OFC IBF stabilization in monolithic quantum dot SML lasers subject to OSI.

Acknowledgment

The authors would like to thank I. Krestnikov for providing the QD wafer, M. Gioannini for helpful discussions, and W. Elsäßer for support.

References

[1] M. L. Davenport, S. Liu, and J. E. Bowers, "Integrated heterogeneous silicon/III-V mode-locked lasers," *Photonon. Res.*, vol. 6, no. 5, pp. 468–478, May 2018.
[2] Z. G. Lu, J. R. Liu, R. J. Poole, C. Y. Song, and S. D. Chang, "Ultra-narrow linewidth quantum dot coherent comb lasers with self-injection feedback locking," *Opt. Exp.*, vol. 26, no. 9, pp. 11909–11914, Apr. 2018.
[3] V. Vujicic *et al.*, "Mitigation of relative intensity noise of quantum dash mode-locked lasers for PAM4 based optical interconnects using encoding techniques," *Opt. Exp.*, vol. 25, no. 1, pp. 20–29, Jan. 2017.
[4] J. N. Kemal *et al.*, "32QAM WDM transmission using a quantum-dash passively mode-locked laser with resonant feedback," in *Proc. Opt. Fiber Commun. Conf. Exhib.*, Mar. 2017, pp. 1–3.
[5] J. Faist *et al.*, "Quantum cascade laser frequency combs," *Nanophotonics*, vol. 5, no. 2, pp. 272–291, 2016.
[6] D. Kazakov *et al.*, "Self-starting harmonic frequency comb generation in a quantum cascade laser," *Nature Photon.*, vol. 11, pp. 789–792, 2017.
[7] S. Liu, D. Jung, J. C. Norman, M. J. Kennedy, A. C. Gossard, and J. E. Bowers, "490 fs pulse generation from passively mode-locked single section quantum dot laser directly grown on on-axis GaP/Si," *Electron. Lett.*, vol. 54, pp. 432–433, Oct. 2018.
[8] Y. Mao, J. Liu, Z. Lu, C. Song, and P. J. Poole, "Femtosecond timing jitter of quantum dot semiconductor comb lasers with self-injection feedback locking," in *Proc. Opt. Fiber Commun. Conf.*, 2019, Art. no. Th2A.8.
[9] Z. G. Lu *et al.*, "High performance InAs/InP quantum dot 34.462-GHz C-band coherent comb laser module," *Opt. Exp.*, vol. 26, no. 2, pp. 2160–2167, Jan. 2018.
[10] C. Weber, L. L. Columbo, M. Gioannini, S. Breuer, and P. Bardella, "Threshold behavior of optical frequency comb self-generation in an InAs/InGaAs quantum dot laser," *Opt. Letters*, vol. 44, no. 14, pp. 3478–3481, Jul. 2019.
[11] Z. G. Lu, J. R. Liu, P. J. Poole, C. Y. Song, and S. D. Chang, "Ultra-narrow linewidth quantum dot coherent comb lasers with self-injection feedback locking," *Opt. Exp.*, vol. 26, no. 9, pp. 11909–11914, Apr. 2018.
[12] Z. Lu *et al.*, "An L-band monolithic InAs/InP quantum dot mode-locked laser with femtosecond pulses," *Opt. Exp.*, vol. 17, no. 16, pp. 13609–13614, Aug. 2009.
[13] R. Rosales *et al.*, "High performance mode locking characteristics of single section quantum dash lasers," *Opt. Exp.*, vol. 20, no. 8, pp. 8649–8657, Apr. 2012.
[14] F. Lelarge *et al.*, "Recent advances on InAs/InP quantum dash based semiconductor lasers and optical amplifiers operating at 1.55 μm," *IEEE J. Sel. Topics Quantum Electron.*, vol. 13, no. 1, pp. 111–124, Jan. 2007.
[15] V. Vujicic *et al.*, "Quantum dash mode-locked lasers for data centre applications," *IEEE J. Sel. Topics Quantum Electron.*, vol. 21, no. 6, pp. 53–60, Nov. 2015.
[16] V. Panapakkam *et al.*, "Amplitude and phase noise of frequency combs generated by single-section InAs/InP quantum-dash-based passively and actively mode-locked lasers," *IEEE J. Quantum Electron.*, vol. 52, no. 11, Nov 2016, Art. no. 1300207.
[17] R. Rosales *et al.*, "InAs/InP quantum-dot passively mode-locked lasers for 1.55 μm applications," *IEEE J. Sel. Topics Quantum Electron.*, vol. 17, no. 5, pp. 1292–1301, Sep./Oct. 2011.
[18] M. Faugeron *et al.*, "High peak power, narrow RF linewidth asymmetrical cladding quantum-dash mode-locked lasers," *IEEE J. Sel. Topics Quantum Electron.*, vol. 19, no. 4, Jul. 2013, Art. no. 1101008.
[19] C. Gosset *et al.*, "Subpicosecond pulse generation at 134 GHz using a quantum-dash-based Fabry-Perot laser emitting at 1.56 μm," *Appl. Phys. Lett.*, vol. 88, Jun. 2006, Art. no. 241105.
[20] K. Merghem, V. Panapakkam, Q. Gaimard, F. Lelarge, and A. Ramdane, "Narrow linewidth frequency comb source based on self-injected quantum-dash passively mode-locked laser," in *Proc. Conf. Lasers Electro-Opt.*, May 2017, pp. 1–2.
[21] K. Sato, "100 GHz optical pulse generation using Fabry-Perot laser under continuous wave operation," *Electron. Lett.*, vol. 37, no. 12, pp. 763–764, Jun. 2001.

[22] C. Calò *et al.*, "Single-section quantum well mode-locked laser for 400 Gb/s SSB-OFDM transmission," *Opt. Exp.*, vol. 23, no. 20, pp. 26442–26449, Oct. 2015.
[23] F. Kefelian, S. O'Donoghue, M. T. Todaro, J. G. McInerney, and G. Huyet, "RF linewidth in monolithic passively mode-locked semiconductor laser," *IEEE Photon. Technol. Lett.*, vol. 20, no. 16, pp. 1405–1407, Aug. 2008.
[24] T. Shimizu, X. Wang, and H. Yokoyama, "Asymmetric colliding-pulse mode-locking in InGaAsP semiconductor lasers," *Opt. Rev.*, vol. 2, no. 6, pp. 401–403, Nov. 1995.
[25] A. R. Rae *et al.*, "Harmonic mode-locking of a quantum-dot laser diode," in *Proc. Ann. Meeting IEEE Lasers Electro-Opt. Society*, Oct. 2006, pp. 874–875.
[26] Y.-C. Xin, Y. Li, V. Kovanis, A. L. Gray, L. Zhang, and L. F. Lester, "Reconfigurable quantum dot monolithic multi-section passive mode-locked lasers," *Opt. Exp.*, vol. 15, no. 12, pp. 7623–7633, Jun. 2007.
[27] Y. Li *et al.*, "Harmonic mode-locking using the double interval technique in quantum dot lasers," *Opt. Exp.*, vol. 18, no. 14, pp. 14637–14643, Jun. 2010.
[28] E. A. Avrutin and E. L. Portnoi, "Suppression of Q-switching instabilities in broadened-waveguide monolithic mode-locked laser diodes," *Opt. Quantum Electron.*, vol. 40, no. 9, pp. 655–664, Jul. 2008.
[29] L. Drzewietzki, S. Breuer, and W. Elsäßer, "Timing phase noise reduction of modelocked quantum-dot lasers by time-delayed optoelectronic feedback," *Electron. Lett.*, vol. 49, pp. 557–559, Apr. 2013.
[30] D. Derickson, A. Mar, and J. Bowers, "Residual and absolute timing jitter in actively mode-locked semiconductor lasers," *Electron. Lett.*, vol. 26, pp. 2026–2028, 1990.
[31] D. J. Derickson, P. A. Morton, J. E. Bowers, and R. L. Thornton, "Comparison of timing jitter in external and monolithic cavity modelocked semiconductor lasers," *Appl. Phys. Lett.*, vol. 59, no. 26, pp. 3372–3374, 1991.
[32] D. Eliyahu, R. A. Salvatore, and A. Yariv, "Noise characterization of a pulse train generated by actively mode-locked lasers," *J. Opt. Soc. Amer. B*, vol. 13, no. 7, pp. 1619–1626, Jul. 1996.
[33] E. Martin *et al.*, "Terahertz-bandwidth coherence measurements of a quantum dash laser in passive and active mode-locking operation," *Opt. Lett.*, vol. 37, no. 23, pp. 4967–4969, Dec. 2012.
[34] R. Arkhipov *et al.*, "Hybrid mode locking in semiconductor lasers: Simulations, analysis, and experiments," *IEEE J. Sel. Topics Quantum Electron.*, vol. 19, no. 4, pp. 1100208, Jul./Aug. 2013.
[35] N. Rebrova, T. Habruseva, G. Huyet, and S. P. Hegarty, "Stabilization of a passively mode-locked laser by continuous wave optical injection," *Appl. Phys. Lett.*, vol. 97, no. 10, 2010, Art. no. 101105.
[36] R. M. Arkhipov *et al.*, "Semiconductor mode-locked lasers with coherent dual-mode optical injection: Simulations, analysis, and experiment," *J. Opt. Soc. Amer. B*, vol. 33, no. 3, pp. 351–359, Mar. 2016.
[37] C. Weber, D. Auth, I. Simos, C. Simos, and S. Breuer, "Repetition rate locking of mutually injected monolithic passively mode-locked semiconductor quantum dot lasers," OSA Technical Digest (online) Optical Society of America, Jun. 2019, Paper CB-P.47.
[38] O. Solgaard and K. Y. Lau, "Optical feedback stabilization of the intensity oscillations in ultrahigh-frequency passively modelocked monolithic quantum-well lasers," *IEEE Photon. Technol. Lett.*, vol. 5, no. 11, pp. 1264–1267, Nov. 1993.
[39] K. Merghem *et al.*, "Low noise performance of passively mode locked quantum-dash-based lasers under external optical feedback," *Appl. Phys. Lett.*, vol. 95, no. 13, 2009, Art. no. 131111.
[40] C. Y. Lin, F. Grillot, Y. Li, R. Raghunathan, and L. F. Lester, "Microwave characterization and stabilization of timing jitter in a quantum-dot passively mode-locked laser via external optical feedback," *IEEE J. Sel. Topics Quantum Electron.*, vol. 17, no. 5, pp. 1311–1317, Sep. 2011.
[41] D. Bimberg, D. Arsenijević, and M. Kleinert, "Jitter reduction by optical feedback of passively mode-locked quantum-dot lasers," in *Proc. IEEE Photon. Conf.*, 2013, pp. 234–235.
[42] S. Breuer *et al.*, "Investigations of repetition rate stability of a mode-locked quantum dot semiconductor laser in an auxiliary optical fiber cavity," *IEEE J. Quantum Electron.*, vol. 46, no. 2, pp. 150–157, Feb. 2010.
[43] L. Drzewietzki, S. Breuer, and W. Elsäßer, "Timing jitter reduction of passively mode-locked semiconductor lasers by self- and external-injection: Numerical description and experiments," *Opt. Exp.*, vol. 21, no. 13, pp. 16142–16161, Jul. 2013.
[44] D. Auth, L. Drzewietzki, C. Weber, A. Klehr, A. Knigge, and S. Breuer, "Repetition rate control of optical self-injected passively mode-locked quantum-well lasers: Experiment and simulation," *Electron. Lett.*, vol. 54, no. 6, pp. 374–376, Mar. 2018.
[45] M. Haji *et al.*, "High frequency optoelectronic oscillators based on the optical feedback of semiconductor mode-locked laser diodes," *Opt. Exp.*, vol. 20, no. 3, pp. 3268–3274, Jan. 2012.
[46] O. Nikiforov, L. Jaurigue, L. Drzewietzki, K. Lüdge, and S. Breuer, "Experimental demonstration of change of dynamical properties of a passively mode-locked semiconductor laser subject to dual optical feedback by dual full delay-range tuning," *Opt. Exp.*, vol. 24, pp. 14301–14310, 2016.
[47] L. Jaurigue, O. Nikiforov, E. Schöll, S. Breuer, and K. Lüdge, "Dynamics of a passively mode-locked semiconductor laser subject to dual-cavity optical feedback," *Phys. Rev. E*, vol. 93, Feb. 2016, Art. no. 022205.
[48] S. Stutz, O. Nikiforov, C. Weber, L. Drzewietzki, T. Walther, and S. Breuer, "Impact of long external fiber cavities on the pulse train stabilization of a passively mode-locked quantum dot laser emitting at 1250 nm," in *Proc. 19th Int. Conf. Transparent Opt. Netw.*, Jul. 2017, pp. 1–4.
[49] B. V. Volovik *et al.*, "Long-wavelength emission in structures with quantum dots formed in the stimulated decomposition of a solid solution at strained islands," *Semiconductors*, vol. 33, no. 8, pp. 901–905, Aug. 1999.
[50] J. Hillbrand *et al.*, "In-phase and anti-phase synchronization in a laser frequency comb," *arXiv: 1908.08504 [physics.optics],*, Aug. 2019.
[51] D. Auth, C. Weber, A. Klehr, A. Knigge, and S. Breuer, "Pulse train timing stability improvement and repetition frequency control of a monolithic mode-locked two-section quantum well semiconductor laser emitting at 1070 nm by all-optical self-feedback configurations," in *Proc. 19th Int. Conf. Transparent Opt. Netw.*, Jul. 2017, pp. 1–4.